Symmetrical Supercapacitor with Graphene-Supported Iron Hexacyanoferrate Electrodes: Wide Potential Window and High Energy Density

Lindiomar Borges de Avila Junior

lindiomarbaj@gmail.com

Universidade Federal de Santa Catarina

Pablo Cesar Serrano Arambulo

Universidade Federal de Santa Catarina

Luis Torres Quispe

National University of Saint Augustine

Adriana Dantas

Universidade Federal de Santa Catarina

Diogo Pontes Costa

Universidade Federal de Santa Catarina

Edy E. Cuevas Arizaca

Universidad Católica de Santa María Arequipa

Diana Patricia Paredes Chávez

Universidad Católica de Santa María Arequipa

Cesar Danial Valdivia Portugal

Universidad Católica de Santa María Arequipa

Christian Klaus Müller

Faculty of Physical Engineering/Computer Sciences, University of Applied Sciences Zwickau, Zwickau, Germany

---

Article

Keywords: Prussian blue, graphene, supercapacitor electrode, high stability, symmetric supercapacitor

Posted Date: January 18th, 2024

DOI: https://doi.org/10.21203/rs.3.rs-3848646/v1

Additional Declarations: No competing interests reported.

Abstract

In this work, iron hexacyanoferrate (FeHCF) particles have been grown onto graphene substrate through pulsed electrodeposition process. Thus, prepared FeHCF electrode exhibits volumetric capacitance of 88 F cm^{-3} (a real capacitance of 26.6 mF cm^{-2}) and high cycling stability with capacitance retention of 93.7% under deep repeating of 10000 galvanostatic charge-discharge cycles in 1M KCl electrolyte. Furthermore, two identical FeHCF electrodes were paired up in order to construct a symmetrical supercapacitor, which delivers a wide potential window of 2 V in 1M KCl electrolyte, and demonstrates large energy density with an offer of high power density.

1. Introduction

As a result of the depletion of fossil fuels and the subsequent rise in air pollution, there is an urgent demand for clean and alternative energy sources. Consequently, significant efforts have been directed towards harnessing sustainable energy sources, such as solar and wind energy systems. Nonetheless, the intermittent nature of these renewable energy sources hinders their substantial impact unless the electricity they generate is efficiently stored. Hence, there arises a critical need to employ advanced energy storage devices to effectively store the energy produced by renewable sources. Supercapacitors, also referred to as electrochemical capacitors, have garnered significant interest as innovative energy storage systems, thanks to their exceptional attributes, such as high-power densities, extended lifespan, and rapid charging capabilities, setting them apart from conventional batteries [1], [2]. The supercapacitor material is the core component of supercapacitor electrodes which largely dictates their electrochemical performance. Variety of electrode materials have been investigated for supercapacitor electrodes, including carbon materials [3], polymeric materials [4], and metal oxides [5]. In 2008, Chen et al. [6] achieved the successful synthesis of three distinct types of transition metal hexacyanoferrates (FeHCF, NiHCF, and CoHCF). These compounds were employed as active electrodes in a supercapacitor operating with a 1M KNO3 electrolyte. Among the tested materials, FeHCF (425 Fg^{-1}), NiHCF (574.7 Fg^{-1}) and CoHCF (261.56 Fg^{-1}) electrodes demonstrated higher discharge capacities at a current density of 0.2 Ag-1. Composites of transition metal hexacyanoferrates with other components have also been used for supercapacitor electrodes.

There are several concerns that need to be further improved in supercapacitors, for example, to extend the working voltage, promote the energy/power densities, long life span, lower the construction cost, and their environmental benign nature [6]. Asymmetric cell configuration is considered an effective way to extend the voltage window of the cell, where positive electrodes (metal oxide-based) and negative electrodes (carbon-based) are generally used [7]. Recent studies have indicated that metal oxide (pseudocapacitive materials) could also be used as the negative electrode in asymmetric supercapacitors [8], [9]. For example, Hu *et al.* [10] have reported Fe_2O_3 nanoparticle cluster/reduced graphene oxide (rGO) paper as a negative electrode which shows improved capacitance in the negative voltage range compared to pristine rGO paper. In another work, Zhang *et al.* [11] have reported MoO_2/MoS_2 as a negative electrode which

shows good electrochemical performance. Nevertheless, designing pseudocapacitive materials as the negative electrode is not simple and often leads to poor electrochemical performance and instability [12]. In 2014, a supercapacitor based on activated carbon showcased remarkable stability during operation, maintaining an unexpectedly high cell voltage of 2.2 V [13]. By manipulating the physicochemical properties of the electrolyte (such as pH or conductivity values) and/or adjusting the surface chemistry of activated carbons, it becomes feasible to elevate the maximum voltage of aqueous supercapacitors. These modifications directly influence the over-potential for water splitting [14]. Aqueous electrolyte-based supercapacitors have garnered attention owing to their favorable attributes, such as relatively high capacitance, excellent power rates, affordability, and eco-friendliness. However, as they are commonly operated in highly corrosive electrolytes, there is a risk of corrosion damage to their closures. To enhance safety, it is preferable to design electrodes suitable for neutral electrolytes [15]. Thus far, only carbonaceous materials and manganese oxide (MnO_2) based electrode materials have shown good electrochemical performance in neutral media [16], [17]. However, some issues persist with these materials, e.g. carbon-based electrodes suffer from relatively low capacitance, and MnO_2-based electrodes are restricted in their cycling stability [18].

The chemical forms (PB and analogs) are described by the general formula $A_x M_y^a \left[M^b (CN)_6 \right]_z$, due to their diverse morphologies and easily controllable size, they have received considerable attention in electrochemical devices, such as electrochemical biosensors [19], [20], Memristors devices [21], [22] and also for supercapacitors [23]–[26]. The open framework structure of FeHCF has wide channels which allow the rapid insertion and removal of electrolyte ions through redox reaction between ferrous and ferric oxidation states in the Fe center [27]–[29]. The rich intercalation chemistry of FeHCF has motivated us to explore this unique material for supercapacitor applications. In this work, we have grown FeHCF particles onto a graphene substrate using pulsed electrodeposition for supercapacitor electrodes. This electrode material shows large volumetric and areal-specific capacitance and ultrahigh cyclic stability in 1M KCl (pH 5) electrolyte. Furthermore, a symmetrical supercapacitor was constructed by pairing up two identical electrodes and achieving a high operating voltage of 2 V with high energy density and power density. In practice, symmetrical supercapacitors are limited to the voltage range of ~ 1.23 V in aqueous electrolytes. To our knowledge, this is the first time that a symmetrical supercapacitor based on FeHCF has achieved 2V cell voltage. Additionally, the low-cost and eco-friendly nature of FeHCF makes this material very attractive for practical application in supercapacitors.

2. Experimental details

First, we prepared graphene film as a conductive substrate onto polyethylene terephthalate (PET) sheet in the following way: the suspension of GO (2 mg mL^{-1}) was mixed with HI (57%) with a volume ratio of 2:0.5. Then the mixture was dropped onto the pre-cleaned PET sheet. After that, the PET sheet was heated up directly by a hot plate at the temperature of 80°C for 3 hours. The obtained graphene films were washed with a copious amount of double distilled water and then ethanol to remove residual iodine. The prepared substrates were preserved for further electrodeposition of FeHCF. The rGO substrates were

electrically contacted by a copper wire and masked to define the area for the electrodeposition of FeHCF. Then, it was immersed in the aqueous electrolyte composed of 0.5 mM of $FeCl_3$, 0.5 mM of $K_3Fe(CN)_6$, 1 M of KCl, and 0.01 M of HCl. The electrochemical deposition of the PB films was performed in potentiostatic mode using an electrochemical workstation (Ivium CompactStat, Eindhoven, Netherlands) as show in Fig. 1. The rGO was used as the working electrode, while the counter and reference electrodes were a platinum foil and a saturated calomel electrode (SCE), respectively. To electroplate Fe-HFC onto rGO substrate, pulses of potential were applied, first a pulse at 0.3 V, followed by pulse at 0 V, -0.3 V and 0 V vs. SCE. All pulses were kept with the same width of 0.1 s. Such a process was done repeatedly 300 times. After this, the samples were washed with water and dried under the stream of nitrogen gas.

The film morphology was analyzed by field emission scanning electron microscopy (FEG-SEM, TESCAN CLARA, Brünn, Czech Republic). The elemental composition was studied with an energy-dispersive x-ray (EDX) detector (Ultim Max 65 SDD, Oxford Instruments, Wiesbaden, Germany) at 15 kV. *The crystallographic film structure was analyzed with a Siemens x-ray diffractometer (D5000, Siemens, München, Germany) using Bragg-Brentano geometry, a Cu Kα x-ray source (λ = 1.5418 Å), equipped with a scintillator detector.*

3. Results and discussion

The structure analysis of as-prepared FeHCF was done by X-ray diffraction as presented in Fig. 2a. Almost all diffraction peaks were indexed to the face-centered Prussian blue structure according to the JCPDS Card No. 52-1907, indicating a crystalline cubic structure of FeHCF particles,, with a lattice constant of a = 10.15 Å (for the 200, 220 and 400 reflexes) in agreement with the literature [30]. The peak at 25° was assigned due to graphene plane stacking diffraction [31]. PB KFe(III)[Fe(II)CN6], or Everitt salt, is the partially reduced counterpart whereby the Fe center coordinated by C has its oxidation state + 2, due to the strong field of the CN ligand. On the other hand, the peripheral cyanide of coordination N, Fe-N, the Fe atoms are in the + 3 oxidation state and with their tetrahedral holes occupied by alkaline cations, Fig. 2b. In Fig. 2c presents a SEM image of electrodeposited FeHCF onto the graphene substrate, one region showing the FeHCF anchored in the rGO (Fig. 2c, left image) and the other with the most agglomerated particles covering the entire electrode (Fig. 2c, right image).

EDX-analysis was performed to determine the layer composition (see Fig. 3). From the EDX spectrum a composition with 42 at% C, 35 at% N, 6 at% O, 12.5 at% Fe, and 4.5 at% Na is obtained. From this amounts, a mixture of 92% $KFe^{3+}[Fe^{2+}(CN)_6]\cdot mH_2O$ and 8% $Fe^{3+}{}_4[Fe^{2+}(CN)_6]_3\cdot mH_2O$ of PB can be proposed based on the found C/N ratio of ~ 1.2 and a Fe/Na ratio of ~ 2.6. The higher amount of C compared with N occurs because of carbon from the graphene and surface contaminations.

The electrochemical performance of FeHCF as a supercapacitor electrode was meticulously assessed through comprehensive cyclic voltammetry (CV) and precise galvanostatic charge-discharge (GCD) measurements, conducted within a sophisticated three-electrode cell system. In this carefully designed setup, a highly conductive 1 M KCl electrolyte was employed, while a Pt foil and saturated calomel

electrode were meticulously chosen as the counter and reference electrodes, respectively, ensuring accurate and reliable characterization of the FeHCF electrode's behavior. In Fig. 4a, a distinct pair of reversible peaks is evident, corresponding to the redox reactions of FeII/III within FeHCF. These reactions are accompanied by the insertion of K + ions to maintain charge neutrality [32]. Furthermore, as the scan rates increase, there is a notable rise in the electrochemical response current. The cyclic voltammetry (CV) curves exhibit a nearly consistent reversible pattern with slight shifts in peak positions, indicating excellent electronic conduction within the electrode. The faradaic transition of PB in the presence of K + ions is proposed as follows [33].

$$Fe^{(III)}_4[Fe^{(II)}(CN)_6]_3 + 4K^+ + 4e^- = K_4Fe^{(II)}_4[Fe^{(II)}(CN)_6]_3$$

For further investigation of the capacitive behavior of the FeHCF electrode, a series of galvanostatic charge-discharge (GCD) measurements were performed at various current densities, as show in Fig. 4b. The discharge curves of the FeHCF electrode displayed a distinct plateau, providing clear evidence of its pseudocapacitive behavior, which aligns closely with the observations from the cyclic voltammetry analysis. Areal and volumetric capacitances of the electrode were calculated from discharge curves at different current densities and results are listed in Table 1. At the highest current density of 3.3 A/cm^3 the charge or discharge step was completed in less than 6 s. To eliminate any potential influence from the graphene substrate as a working electrode, we conducted charge-discharge measurements on both the pure graphene substrate and the FeHCF/graphene substrate, under identical conditions. The experiments were carried out at a current density of 0.33 A/cm3. The results revealed a significantly lower capacitance for the pure graphene substrate, as illustrated in Fig. 4c. The cyclic stability of the electrode materials is another important parameter in the selection of supercapacitor electrode. The cycling stability of the FeHCF was performed under repetitive GCD cycles at the constant current density of 0.33 A cm^{-3}. The variation of capacitance with cycle number is shown in Fig. 4d. From the start, a gradual decrease in capacitance was noticed and later a sharp increase in capacitance was observed after 2500 cycles, which can be explained as the activation process of the electrode material. The long span of the charging-discharging process may help electrolyte ions intercalate into the open framework structure of FeHCF nanoparticles, fully utilizing the elective surface area of electrode materials. After repeating 10000 GCD cycles, more than 93% capacitance was retained from its initial one, indicating the ultrahigh stability of the electrode materials in 1M KCl electrolyte (pH ~ 5). This long-term cyclic stability of FeHCF is probably due to the strong interaction of FeHCF nanoparticles at the interface of the graphene substrate. Cycling stability behavior is the foremost metric determining the success of supercapacitor electrode materials. The inset of Fig. 4d shows that the GCD curves taken after 1000, 2000, 3000, 5000, 8000, and 10000 cycles, have no significant change in the symmetry of charge and discharge curves after consecutively repeating cycles. Again the electrode material is demonstrating a long-term reliability of the electrochemical performance. The stability of the electrode materials is also dependent on the choice of electrolyte. Generally, Prussian blue analogues are known to be more stable in acidic electrolytes than in neutral and basic media. The above findings reveal that FeHCF nanoparticles have large specific capacitance and excellent cycling reliability in KCl electrolyte at ~ pH 5.

Table 1
Areal and volumetric capacitance of FeHCF at different current densities

Area spec. current density ($mA\ cm^{-2}$)	Area spec. capacitance ($mF\ cm^{-2}$)	Volumetric spec. current density ($A\ cm^{-3}$)	Area spec. capacitance ($F\ cm^{-3}$)
0.02	26.6	0.06	88.0
0.06	17.1	0.19	63.0
0.10	14.0	0.33	46.4
0.16	12.8	0.52	37.2
0.20	8.5	0.66	23.7
0.60	6.3	1.98	15.8
1.00	3.9	3.30	12.3

The symmetrical supercapacitor was mounted as shown in Fig. 5a. Before the pairing of two identical electrodes with the same shape and size, we first tested FeHCF electrode in negative and positive potential windows under different potential ranges in a three electrodes cell setup and at a scan rate of 100 mV/s. As shown in Fig. 5b, the CV curves of FeHCF electrode exhibit a rectangular shape without any redox peaks in negative potential region, which is indicating pure capacitive behavior. The rectangular shape of the pseudocapacitive materials in the negative windows have also been shown in earlier reported works [34]. The mechanism of rectangular CV curve for metal oxides in the negative windows is not fully clear. However, to rule out the capacitive behavior of FeHCF electrode in the negative potential window, we measured the CV of graphene substrate without FeHCF from − 0 to -1V. The CV curve of pure graphene substrate was smaller than FeHCF; this means that graphene substrate has a lower capacitance than FeHCF coated graphene substrate in the negative potential window (Fig. 5b). Thus, it is clear that FeHCF the additional capacitance is arising from FeHCF showing typical electrical double-layer capacitance behavior in negative potential windows with KCl electrolyte. Furthermore, the current leap of FeHCF electrode at the negative end (~ 1V) of the potential window increases sharply which indicates hydrogen evaluation in the KCl electrolyte. A sharp increase in current for the FeHCF electrode near to ~ 1V, is due to the oxygen evaluation on the electrode.

According to the performance of FeHCF in negative and positive potential windows in three electrode cell configuration, a symmetrical supercapacitor (two-electrode cell system) was made up by pairing two identical electrodes of FeHCF separated by filter paper in aqueous 1M KCl electrolyte. The symmetrical supercapacitor system was operated by cyclic voltammetry over a wide voltage range of 0–2 V at a constant scan rate of 50 mV/s as shown in Fig. 5c. Figure 5d shows the CVs of the full cell between 0 and 2V at various scan rates. The capacities of a symmetrical supercapacitor of 49.5 F cm^{-3} at a current

density of 0.16 A cm^{-3}, and 6.4 F cm^{-3} at current density of 3.3 A cm^{-3} were recorded from the discharge curve as shown in Fig. 5e. It is worth mentioning that our symmetrical supercapacitor successfully achieved 2V of the voltage window in two electrode cell configurations. Most of the symmetrical supercapacitors are limited to voltage range of ~ 1 V [34], [35]. Only recently, Xia et al. [36] developed a high-voltage symmetric RuO_2//RuO_2 supercapacitor that gives a cell voltage of up to 1.6 V.

The device prepared herein demonstrates the energy density of 27.5 mWh cm^{-3} at the power density of 330 W cm^{-3} and the energy density can be maintained at 9.3 mWh cm^{-3} with a power density of 12600 W cm^{-3} (Fig. 5f). This characteristic is notable in that high-power density can be simultaneously achieved along with high specific energy, thus making these materials very promising for high-energy storage supercapacitors. The impressive electrochemical performance of the FeHCF electrode material in the aqueous electrolyte may be ascribed to the following factors: first the open framework of FeHCF contains large interstitial sites which can host large amounts of potassium ions that can be transported within the channels. Second, the high ionic conductivity of the aqueous electrolyte may facilitate the fast-ionic transport between the electrolyte and the electrode.

4. Conclusion

In summary, iron hexacyanoferrate nanoparticles have been grown onto graphene substrate using pulsed electrodeposition and used as a supercapacitor electrode. The electrode demonstrates exceptional electrochemical performance, excelling in both capacitance and stability aspects.This electrode delivers a high volumetric capacitance of 88 F cm^{-3} (areal capacitance of 26.6 mF cm^{-2}) and maintains the capacitance at about 93.7% after repeating 10000 galvanostatic charge-discharge cycles in 1M KCl electrolyte. When two identical electrodes of FeHCF were paired up in the form of a symmetrical supercapacitor, it achieved a high operating voltage window of 2V. To our knowledge, this is the highest voltage window reported for symmetrical supercapacitor in aqueous electrolyte, so far. Moreover, the symmetrical supercapacitor shows an energy density of 27.5 mWh cm^{-3} at a power density of 330 W cm^{-3}.

Declarations

Acknowledgement

We acknowledge the financial support of CAPES Govt. of Brazil to carry out this research work, and Vicerrectorado de Investigación Universidad Católica de Santa María. The authors thanks for funding Resolution No 29002-R-2022.

Author contributions

LBA contributed to - data acquisition and writing – original draft. PAS was involved in review and editing. LTQ contributed to review and editing. AD was involved in review and editing. DPC contributed to review

and editing. EECA was involved in review – editing and funding acquisition. DPPC was involved in review – editing and funding acquisition. CDVP was involved in review – editing and funding acquisition. CKM contributed to supervision – review and editing. All authors have commented on previous editions of the manuscript. All authors read and approved the final draft.

Conflict of interest. The authors declare that they have no known competing interests or conflicts of interest of any kind.

Data availability

The datasets produced or analyzed during the present study are not publicly available, as they also form a part of an ongoing investigation. However, they are available from the corresponding author upon reasonable request.

Supplementary information

Not Applicable

Ethical approval

Not applicable

References

1. E. S. Goda, S. Lee, M. Sohail, and K. R. Yoon, “Prussian blue and its analogues as advanced supercapacitor electrodes,” J. Energy Chem., vol. 50, pp. 206–229, 2020, doi: 10.1016/j.jechem.2020.03.031.
2. Z. Tang *et al.*, “Fabrication of various metal hexacyanoferrates@CNF through acid-regulation for high-performance supercapacitor with superior stability,” Carbon N. Y., vol. 187, pp. 47–55, Feb. 2022, doi: 10.1016/j.carbon.2021.10.076.
3. Y. Wang *et al.*, “Recent progress in carbon-based materials for supercapacitor electrodes: a review,” J. Mater. Sci., vol. 56, no. 1, pp. 173–200, Jan. 2021, doi: 10.1007/s10853-020-05157-6.
4. C. A. Amarnath and S. N. Sawant, “Tailoring synthesis strategies for polyaniline-prussian blue composite in view of energy storage and H2O2 sensing application,” Electrochim. Acta, vol. 295, pp. 294–301, Feb. 2019, doi: 10.1016/j.electacta.2018.10.132.
5. L. Zhang, H. Bin Wu, S. Madhavi, H. H. Hng, and X. W. (David) Lou, “Formation of Fe_2O_3 Microboxes with Hierarchical Shell Structures from Metal–Organic Frameworks and Their Lithium Storage Properties,” *J. Am. Chem. Soc.*, vol. 134, no. 42, pp. 17388–17391, Oct. 2012, doi: 10.1021/ja307475c.
6. S. A. A. Shah, R. Idrees, and S. Saeed, “A critical review on polyimide derived carbon materials for high-performance supercapacitor electrodes,” J. Energy Storage, vol. 55, p. 105667, Nov. 2022, doi: 10.1016/j.est.2022.105667.

7. Y. Gao and L. Zhao, “Review on recent advances in nanostructured transition-metal-sulfide-based electrode materials for cathode materials of asymmetric supercapacitors,” Chem. Eng. J., vol. 430, p. 132745, Feb. 2022, doi: 10.1016/j.cej.2021.132745.
8. Y. Shao *et al.*, “Design and Mechanisms of Asymmetric Supercapacitors,” Chem. Rev., vol. 118, no. 18, pp. 9233–9280, Sep. 2018, doi: 10.1021/acs.chemrev.8b00252.
9. Lichchhavi, A. Kanwade, and P. M. Shirage, “A review on synergy of transition metal oxide nanostructured materials: Effective and coherent choice for supercapacitor electrodes,” J. Energy Storage, vol. 55, p. 105692, Nov. 2022, doi: 10.1016/j.est.2022.105692.
10. Y. Hu, C. Guan, Q. Ke, Z. F. Yow, C. Cheng, and J. Wang, “Hybrid Fe_2O_3 Nanoparticle Clusters/rGO Paper as an Effective Negative Electrode for Flexible Supercapacitors,” *Chem. Mater.*, vol. 28, no. 20, pp. 7296–7303, Oct. 2016, doi: 10.1021/acs.chemmater.6b02585.
11. T. Zhang *et al.*, “Design and preparation of MoO 2 /MoS 2 as negative electrode materials for supercapacitors,” *Mater. Des.*, vol. 112, pp. 88–96, Dec. 2016, doi: 10.1016/j.matdes.2016.09.054.
12. P. Bhojane, “Recent advances and fundamentals of Pseudocapacitors: Materials, mechanism, and its understanding,” J. Energy Storage, vol. 45, p. 103654, Jan. 2022, doi: 10.1016/j.est.2021.103654.
13. K. Fic, M. Meller, and E. Frackowiak, “Strategies for enhancing the performance of carbon/carbon supercapacitors in aqueous electrolytes,” Electrochim. Acta, vol. 128, pp. 210–217, May 2014, doi: 10.1016/j.electacta.2013.11.047.
14. B. Pal, S. Yang, S. Ramesh, V. Thangadurai, and R. Jose, “Electrolyte selection for supercapacitive devices: a critical review,” Nanoscale Adv., vol. 1, no. 10, pp. 3807–3835, 2019, doi: 10.1039/C9NA00374F.
15. W. Ye, H. Wang, J. Ning, Y. Zhong, and Y. Hu, “New types of hybrid electrolytes for supercapacitors,” *J. Energy Chem.*, vol. 57, pp. 219–232, Jun. 2021, doi: 10.1016/j.jechem.2020.09.016.
16. N. Hillier, S. Yong, and S. Beeby, “The good, the bad and the porous: A review of carbonaceous materials for flexible supercapacitor applications,” Energy Reports, vol. 6, pp. 148–156, May 2020, doi: 10.1016/j.egyr.2020.03.019.
17. T. Yue, B. Shen, and P. Gao, “Carbon material/MnO2 as conductive skeleton for supercapacitor electrode material: A review,” Renew. Sustain. Energy Rev., vol. 158, p. 112131, Apr. 2022, doi: 10.1016/j.rser.2022.112131.
18. S. Kumar, G. Saeed, L. Zhu, K. N. Hui, N. H. Kim, and J. H. Lee, “0D to 3D carbon-based networks combined with pseudocapacitive electrode material for high energy density supercapacitor: A review,” Chem. Eng. J., vol. 403, p. 126352, Jan. 2021, doi: 10.1016/j.cej.2020.126352.
19. J. Li, X. Yan, X. Li, X. Zhang, and J. Chen, “A new electrochemical immunosensor for sensitive detection of prion based on Prussian blue analogue,” Talanta, vol. 179, pp. 726–733, Mar. 2018, doi: 10.1016/j.talanta.2017.12.006.
20. J. Liu *et al.*, “Zinc-modulated Fe–Co Prussian blue analogues with well-controlled morphologies for the efficient sorption of cesium,” J. Mater. Chem. A, vol. 5, no. 7, pp. 3284–3292, 2017, doi: 10.1039/C6TA10016C.

21. L. B. Avila, P. C. Serrano Arambulo, A. Dantas, E. E. Cuevas-Arizaca, D. Kumar, and C. K. Müller, “Study on the Electrical Conduction Mechanism of Unipolar Resistive Switching Prussian White Thin Films,” Nanomaterials, vol. 12, no. 16, p. 2881, Aug. 2022, doi: 10.3390/nano12162881.
22. L. B. Avila *et al.*, “Resistive switching in electrodeposited Prussian blue layers,” Materials (Basel)., vol. 13, no. 24, pp. 1–11, 2020, doi: 10.3390/ma13245618.
23. M. J. Piernas Muñoz and E. Castillo Martínez, “Electrochemical Performance of Prussian Blue and Analogues in Aqueous Rechargeable Batteries,” in Prussian Blue Based Batteries, 2018, pp. 23–44. doi: 10.1007/978-3-319-91488-6_3.
24. J. Nai and X. W. (David) Lou, “Hollow Structures Based on Prussian Blue and Its Analogs for Electrochemical Energy Storage and Conversion,” *Adv. Mater.*, vol. 31, no. 38, p. 1706825, Sep. 2019, doi: 10.1002/adma.201706825.
25. S. Zhao *et al.*, “The Rise of Prussian Blue Analogs: Challenges and Opportunities for High-Performance Cathode Materials in Potassium-Ion Batteries,” Small Struct., vol. 2, no. 1, p. 2000054, Jan. 2021, doi: 10.1002/sstr.202000054.
26. C. Xu *et al.*, “Prussian Blue Analogues in Aqueous Batteries and Desalination Batteries,” Nano-Micro Lett., vol. 13, no. 1, p. 166, Dec. 2021, doi: 10.1007/s40820-021-00700-9.
27. A. Zhou *et al.*, “Hexacyanoferrate-Type Prussian Blue Analogs: Principles and Advances Toward High-Performance Sodium and Potassium Ion Batteries,” Adv. Energy Mater., vol. 11, no. 2, p. 2000943, Jan. 2021, doi: 10.1002/aenm.202000943.
28. Y. Li *et al.*, “Prussian blue analogs cathodes for aqueous zinc ion batteries,” Mater. Today Energy, vol. 29, p. 101095, Oct. 2022, doi: 10.1016/j.mtener.2022.101095.
29. Y. Lin, L. Zhang, Y. Xiong, T. Wei, and Z. Fan, “Toward the Design of High-performance Supercapacitors by Prussian Blue, its Analogues and their Derivatives,” *ENERGY Environ. Mater.*, vol. 3, no. 3, pp. 323–345, Sep. 2020, doi: 10.1002/eem2.12096.
30. H. J. Buser, D. Schwarzenbach, W. Petter, and A. Ludi, “The crystal structure of Prussian Blue: Fe4[Fe(CN)6]3.xH2O,” *Inorg. Chem.*, vol. 16, no. 11, pp. 2704–2710, Nov. 1977, doi: 10.1021/ic50177a008.
31. M. Khalid, M. A. Tumelero, and A. A. Pasa, “Asymmetric and symmetric solid-state supercapacitors based on 3D interconnected polyaniline-carbon nanotube framework,” RSC Adv., vol. 5, no. 76, pp. 62033–62039, 2015, doi: 10.1039/c5ra11256g.
32. C. D. Wessells, R. A. Huggins, and Y. Cui, “Copper hexacyanoferrate battery electrodes with long cycle life and high power,” *Nat. Commun.*, vol. 2, no. 1, p. 550, Sep. 2011, doi: 10.1038/ncomms1563.
33. K. Itaya, T. Ataka, and S. Toshima, “Spectroelectrochemistry and Electrochemical Preparation Method of Prussian Blue Modified Electrodes,” J. Am. Chem. Soc., vol. 104, no. 18, pp. 4767–4772, 1982, doi: 10.1021/ja00382a006.
34. J. Huang *et al.*, “Hierarchical porous carbon with network morphology derived from natural leaf for superior aqueous symmetrical supercapacitors,” *Electrochim. Acta*, vol. 258, pp. 504–511, Dec. 2017, doi: 10.1016/j.electacta.2017.11.092.

35. H. Li *et al.*, “Intertwined carbon networks derived from Polyimide/Cellulose composite as porous electrode for symmetrical supercapacitor,” J. Colloid Interface Sci., vol. 609, pp. 179–187, Mar. 2022, doi: 10.1016/j.jcis.2021.11.188.
36. H. Xia, Y. Shirley Meng, G. Yuan, C. Cui, and L. Lu, “A Symmetric RuO2/RuO2 Supercapacitor Operating at 1.6 V by Using a Neutral Aqueous Electrolyte,” Electrochem. Solid-State Lett., vol. 15, no. 4, p. A60, 2012, doi: 10.1149/2.023204esl.

Figures

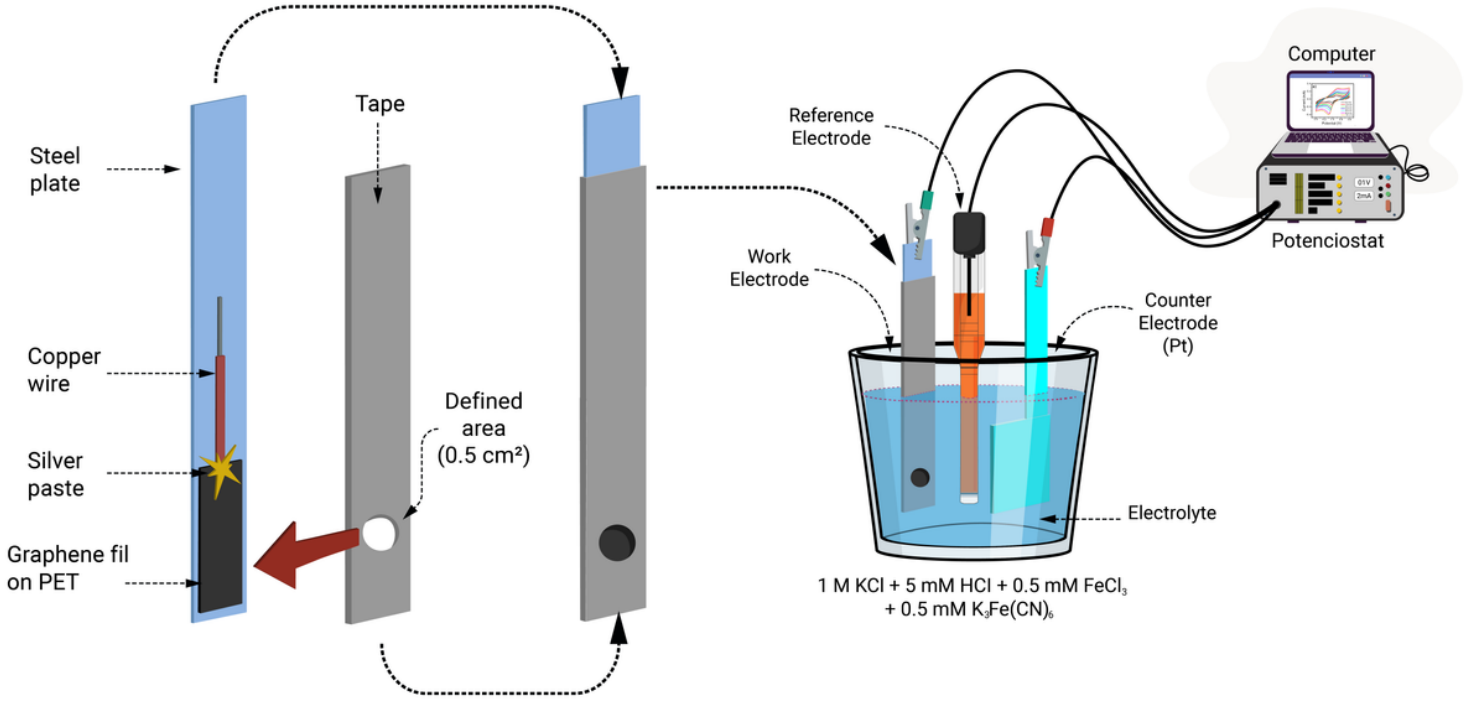

Figure 1

Schematic illustration of electrocoating of FeHCF onto graphene substrate.

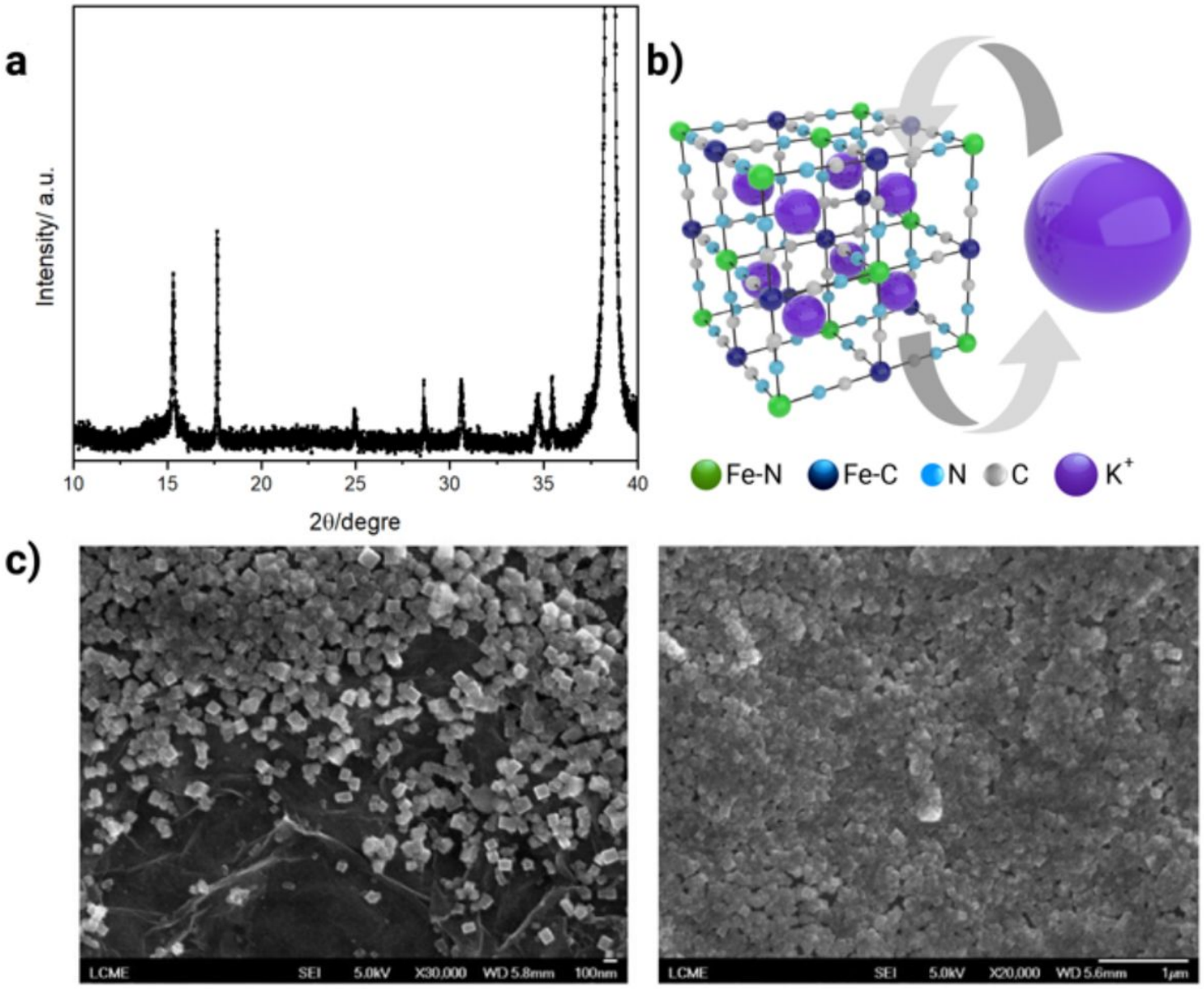

Figure 2

Structure and morphology of FeHCF. a) comparison of XRD pattern of FeHCF nanoparticles with simulated cubic $Fe_4[Fe(CN)_6]$, b) demonstration of unit cell of cubic FeHCF and insertion/exertion of K^+ ion, and c) SEM images of as prepared FeHCF nanoparticles onto graphene substrate.

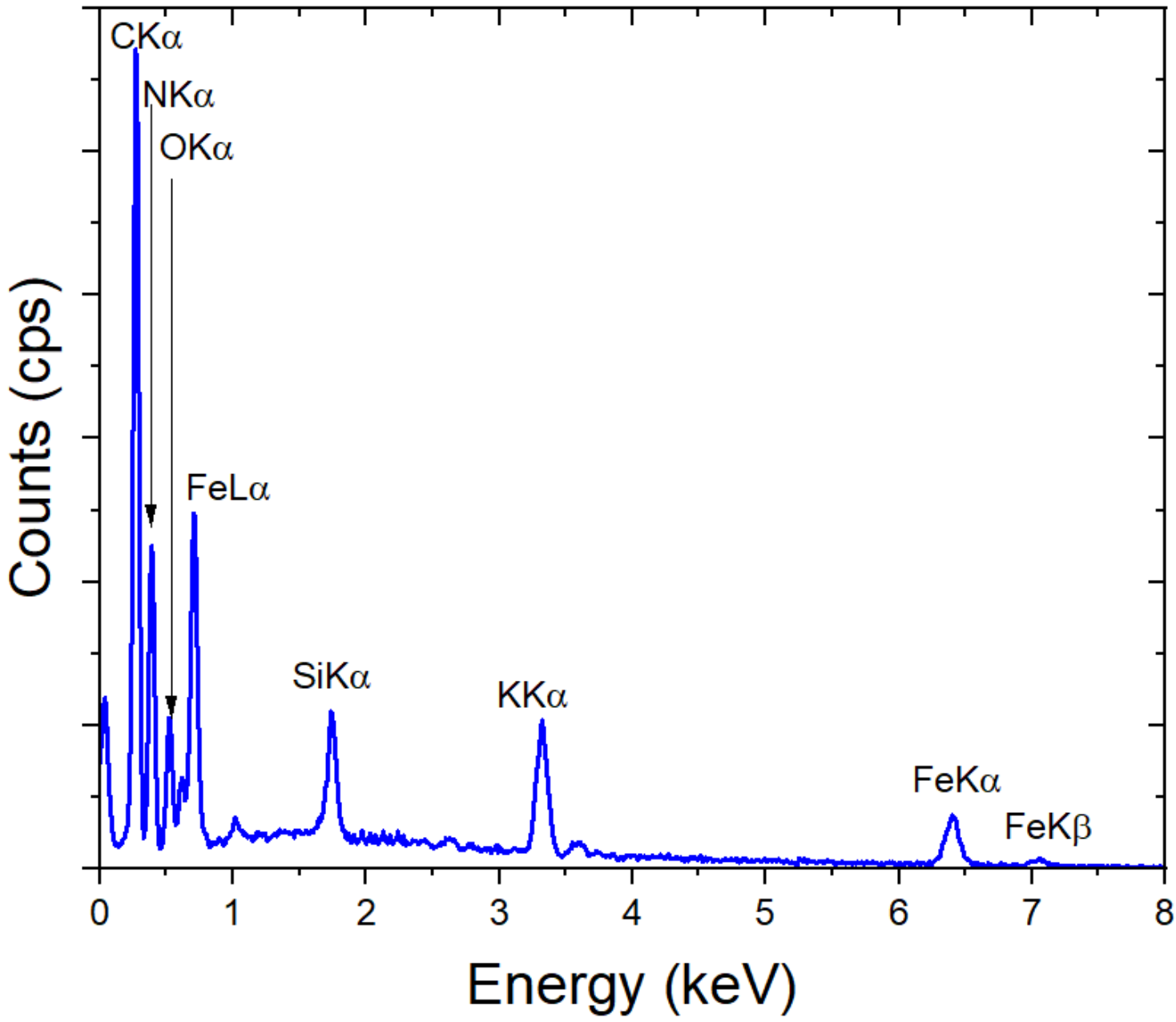

Figure 3

EDX analysis of FeHCF measured at 15 keV.

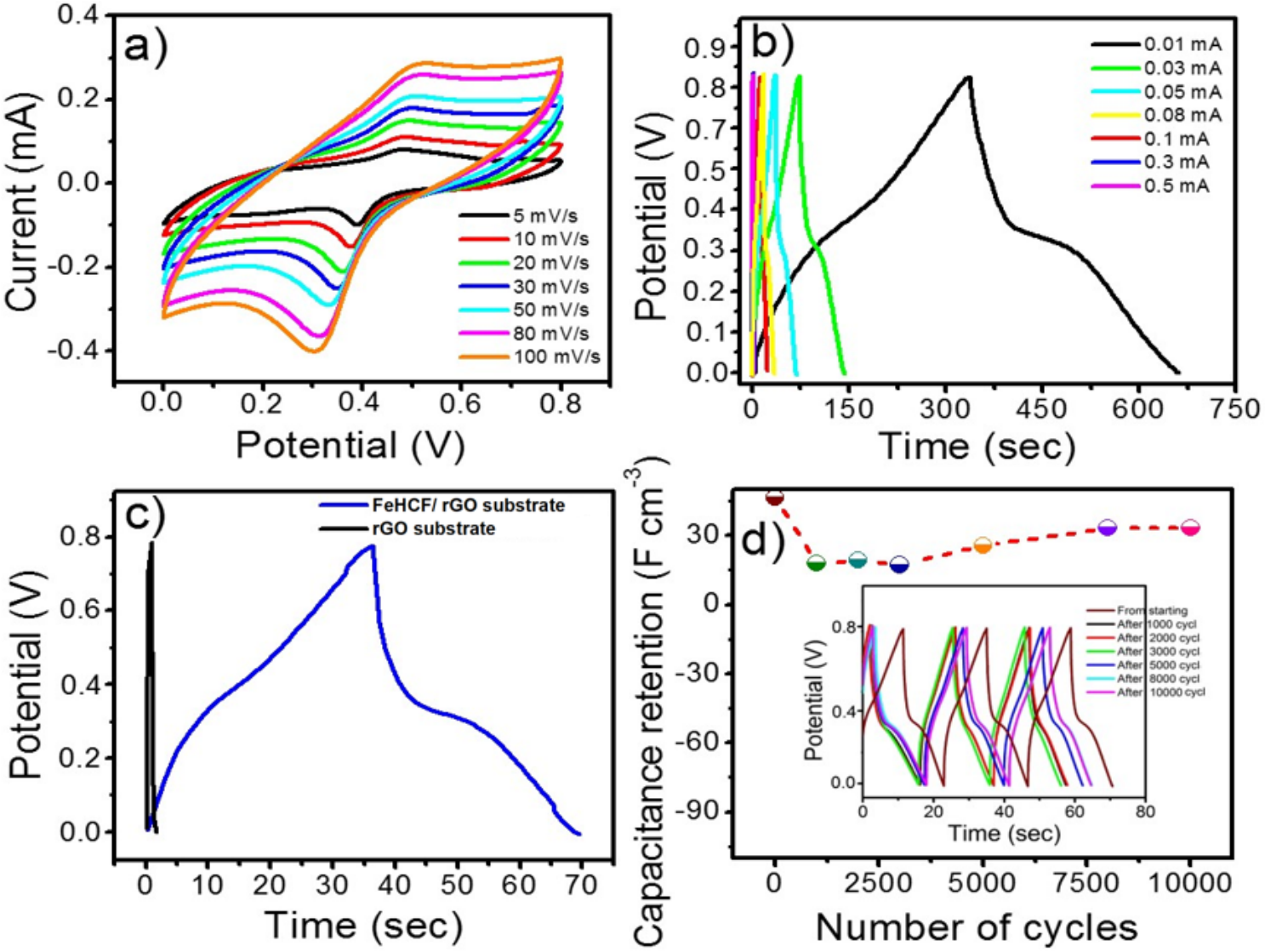

Figure 4

Electrochemical characterization of FeHCF electrode in negative and positive potential range in three electrode cell system. a) cyclic voltammogram curves of FeHFC onto graphene substrate at different potential range in negative and positive region at 100 mV/s scan rates, b) galvanostatic charge-discharge curves at different current densities, c) difference in charge-discharge curve of bare graphene substrate and FeHCF/ reduced graphene substrate at 0.33 A cm^{-3}, and d) cycling behavior of FeHCF electrode at different cycle numbers at 0.66 A cm^{-3} (inset shows the charge-discharge curve right after taken at different hundreds of cycles).

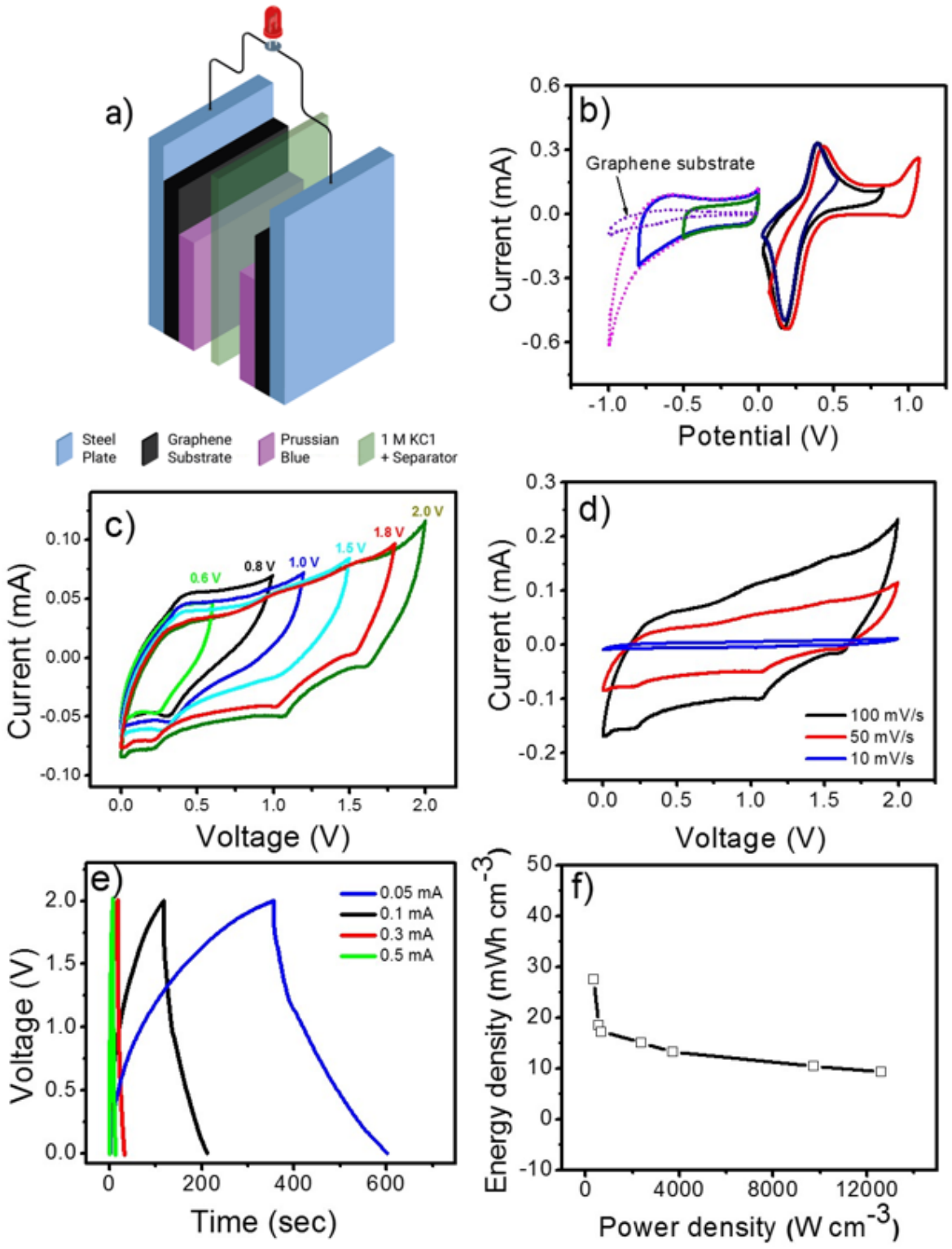

Figure 5

Symmetrical supercapacitor performance. a) schematic illustration of the fabricated symmetrical supercapacitor device, b) cyclic voltammogram behavior of graphene substrate alone as well as FeHCF onto graphene substrate in negative and positive potential windows, c) cyclic voltammogram curves of symmetrical supercapacitor at different voltage windows, d) CV curves of symmetrical supercapacitor at

different scan rate in a 2V voltage window, e) galvanostatic charge-discharge curves at different current densities, and f) Ragone plot, energy density versus power density.